

Article

Nanomaterial Sensing Advantages: Electrochemical Behavior, Optimization and Performance of f-MWCNTs/CS/PB/AuE towards Aluminum Ions (Al^{3+}) in Drinking Water

Gilbert Ringgit ¹, Shafiquzzaman Siddiquee ^{1,*} , Suryani Saallah ¹ and Mohammad Tamrin Mohamad Lal ² ¹ Biotechnology Research Institute, Universiti Malaysia Sabah, Kota Kinabalu 88400, Sabah, Malaysia² Borneo Research Marine Institute, Universiti Malaysia Sabah, Kota Kinabalu 88400, Sabah, Malaysia

* Correspondence: shafiqpab@ums.edu.my

Abstract: Modern technology has been evolving towards nanotechnology due to the materials that can be transformed and manipulated on micro and nanoscales. In terms of detection, nanomaterials offer substantial sensing advantages, particularly in terms of enhanced sensitivity, synergistic effect, stability and selectivity. The immobilization of nanoparticles could alter the physicochemical properties of the electrode's surface depending on the type of materials synthesized and employed. This research examined the synthesis of multiwalled carbon nanotubes (MWCNTs) and chitosan (CS), as well as the immobilization of Prussian blue (PB) on the surface of a bare gold electrode (AuE). These materials have been reported to have strong electrical conductivity and nanomaterial compatibility. In contrast, aluminum has been described as a replacement for traditional water quality treatment processes, such as chlorination and ozonation. Aluminum concentrations must be monitored despite the use of chemical treatment for water quality. Hence, excessive levels of exposure frequently result in neurotoxic effects including Alzheimer's and Parkinson's disorders. In this experiment, the optimal conditions for f-MWCNTs, CS, PB, and AuE for the detection of Al^{3+} are phosphate-buffered saline (PBS) (0.1 M, pH 2) with 5 mM Prussian Blue; scan rate = 0.25 Vs^{-1} ; accumulation duration = 25 s; and volume = 10 mL (ratio of 4:6). The performance of f-MWCNTs, CS, PB, and AuE was measured between 0.2 and 1 ppm with a correlation coefficient of $R^2 = 0.9853$ ($y = 0.0387x + 0.0748$). The limit of detection (LOD) of the modified electrode was determined to be 0.002 ppm, with a recovery of 98.66–99.56%. The application of nanoparticles resulted in various advantages, including high conductivity, a simple, less time-consuming preparation technique, and enhanced sensitivity and stability for detecting the lowest concentration of Al^{3+} in drinking water.

Keywords: aluminum ions; functionalized multi-walled carbon nanotubes; chitosan; Prussian blue; drinking water



Citation: Ringgit, G.; Siddiquee, S.; Saallah, S.; Mohamad Lal, M.T. Nanomaterial Sensing Advantages: Electrochemical Behavior, Optimization and Performance of f-MWCNTs/CS/PB/AuE towards Aluminum Ions (Al^{3+}) in Drinking Water. *Crystals* **2023**, *13*, 497. <https://doi.org/10.3390/cryst13030497>

Academic Editors: Mohamed A. Tahoon and Abdelfattah Amari

Received: 8 February 2023

Revised: 6 March 2023

Accepted: 8 March 2023

Published: 14 March 2023



Copyright: © 2023 by the authors. Licensee MDPI, Basel, Switzerland. This article is an open access article distributed under the terms and conditions of the Creative Commons Attribution (CC BY) license (<https://creativecommons.org/licenses/by/4.0/>).

1. Introduction

The trivalent metal ion aluminum (Al^{3+}) is the third most abundant metallic element in the Earth's crust [1,2]. Aluminum is the second most commonly used element in the transportation, electronics, building structure, water treatment, pharmaceutical, and packaging industries [3]. Aluminum is a part of the chemical treatment that used in water treatment processes (chlorination and ozonation) [2]. Bromide has a carcinogenic effect on animals, raises the pH of water, and decreases the concentration of organic substances [4]. Aluminum's applications in daily life including antiperspirants, deodorants, cookware, cans, and bleaching. Thus, the amount of aluminum entering the body cannot be predicted. Aluminum is believed to be primarily consumed through drinking water [5]. Aluminum has been recognized as a neurotoxic (Alzheimer's and Parkinson's disease) to humans over the past century [6]. Other harmful consequences of excessive consumption included kidney dysfunction, osteomalacia, and breast cancer [1,6,7]. Aluminum levels in drinking water should not exceed 0.2 parts per million

(ppm) [8]. In water, the physical features of heavy metal pollutants such as aluminum are clear and invisible [9,10]. To date, the identification of aluminum, methods such as spectrometry [11,12], spectroscopy [13,14], UV–vis analysis [15], neutron activation analysis [16] and high-performance liquid chromatography [17] have been utilized despite their limitations. The disadvantages of these technologies, including specialist handling, high operational costs, and long analysis [7,18]. The electrochemical method is, to the best of our knowledge, the most effective technique for detecting aluminum ions due to its high sensitivity, rapid analysis, and cost effectiveness [18,19].

In order to detect the lowest target concentration, nanoparticles must be present on the surface of the electrode using the electrochemical approach. Previous studies have utilized multiwalled carbon nanotubes (MWCNTs) and chitosan (CS) to detect trace metals [20,21], analyze energy gaps [22], measure hormones [23,24], engineer tissues [25,26], produce medicinal food [27], and test pharmaceuticals [28,29]. CS is a polymer that consists of D-glucosamine and N-acetyl-d-glucosamine and is the second most abundant natural polymer after cellulose, according to Janegitz et al. [21]. Polysaccharides are the natural polymer in CS [7]. CS is non-toxic, biocompatible, biodegradable, and has low immunogenicity due to the presence of functional amino and hydroxyl groups [22]. Chemical cross-linking can enhance the adsorption process and ion selectivity, and in the presence of CS, the adhesion and compatibility qualities of MWCNTs may be improved [20]. MWCNTs have widespread applications due to their excellent electrical conductivity and chemical stability [28], high electron transfer rate [20], and chemical and biological functional groups [25]. Recently, various modifications of MWCNTs and CS have been used to detect vanillin and tartrazine [30], chloramphenicol, glucose, acetaminophen, p-aminophenol, and tryptophan [31].

Prussian Blue (PB) is composed of $\text{Fe}_4[\text{Fe}(\text{CN})_6]^{3-}$ and is used to detect chemical contamination. PB was used to detect H_2O_2 in the presence of oxygen molecules with excellent selectivity [32]. Yang et al. [33] also reported that PB was applied to the detection of organic chemicals in human serum and improved the performance of the electrochemical sensor due to an electrocatalytic reaction. The formation of the current signal by the analyte was investigated using cyclic voltammetry (CV) and differential pulse voltammetry (DPV). The electrochemical behaviors of oxidation and reduction production under a given potential range were investigated using the CV optimization method [34]. The DPV approach was applied to performance analysis by measuring the formation of surface complexes and the sensitivity of the modified electrode to target ions [35].

The focus of this study is the synthesis of a modified gold electrode (f-MWCNTs/CS/PB/AuE) for the detection of Al^{3+} using nanomaterials such as chitosan and functionalized multi-walled carbon nanotubes supported by Prussian blue. The modification of chitosan with functionalized multi-walled carbon nanotubes and immobilized Prussian blue resulted in the detection of Al^{3+} below the safety level, generating excellent cyclic voltammetry (CV) signals under optimal conditions. Prior to its application in detecting Al^{3+} in drinking water, the performance of f-MWCNTs/CS/PB/AuE was evaluated using the differential pulse voltammetry (DPV) method.

2. Materials and Methods

2.1. Reagents and Chemicals

Phosphate-buffered saline (PBS) was prepared using the method described by Jeon et al. [36], with some modifications. Specifically, 0.1 M of dipotassium hydrogen phosphate (K_2HPO_4), potassium dihydrogen phosphate (KH_2PO_4), and sodium chloride (NaCl) were dissolved in deionized milli-Q (Millipark[®] 40) water. Prussian blue, a redox indicator, was prepared by mixing potassium ferrocyanide(II) trihydrate and iron (III)chloride purchased from Sigma-Aldrich (St. Louis, MO, USA) [37]. Chitosan (CS) and multiwalled carbon nanotubes (MWCNTs) were purchased from Sigma-Aldrich (USA). Aluminum sulphate (Al_3SO_4), a target ion, was purchased from System Chemicals, Malaysia. Other chemicals used in the experiments were of standard reagent grade and

were diluted with milli-Q (Millipark® 40) water. The experiments were conducted at a temperature of 21.0 ± 2.0 °C.

2.2. Instrumentations

All electrochemical measurements were carried out using a potentiostat/galvanostat (PGSTAT302N, serial number: AUT85150, Utrecht, The Netherlands) electrochemical workstation (Metrohm-Autolab B.V) with a standard three-electrodes system consisting of a 3 mm diameter of bare gold electrode (AuE), platinum wire (Pt), and silver/silver chloride (Ag/AgCl) as the working, counter, and reference electrodes (Metrohm Autolab, Utrecht, The Netherlands), respectively. Voltammogram analysis was obtained from the cyclic voltammetry (CV) and differential pulse voltammetry (DPV) in NOVA Autolab 1.11 software (version 1.11.0). All the experiments were performed with 10 mL of analytical buffer (0.1 M) in an electrochemical cell at room temperature conditions of 21.0 ± 2.0 °C. The characterization of nanomaterials was observed under scanning electron microscopy (SEM) (Hitachi S-3400N, Schaumburg, IL, USA) and transmission electron microscopy (TEM) (FEI Tecnai G2 Spirit BioTWIN, Hillsboro, OR, USA). The pH was measured using a pH meter (Model: pH 2700 Eutech Instrument, Landsmeer, The Netherlands). Digital electronic microbalance (model: TLE204E Mettler Toledo, Columbus, OH, USA) was used to measure the weight of the chemicals and reagents throughout the whole experiments.

2.3. Functionalization of Multiwalled Carbon Nanotubes (f-MWCNTs)

Functionalization of multiwalled carbon nanotubes (f-MWCNTs) was performed with modifications according to Shalauddin et al. [28]. Briefly, multiwalled carbon nanotubes were functionalized by dissolving 1 g of MWCNTs powder in a 3 to 1 solution of strong sulfuric acid (H_2SO_4) and nitric acid (HNO_3). The mixture was stirred under a fume hood for 3 h. To maintain a neutral pH, the homogenized mixture was rinsed with a substantial quantity of distilled water. The mixture's pH was determined using a pH meter. The mixed solution was then removed, and the dark precipitate of f-MWCNTs was dried at 60 °C for 24 h. The f-MWCNTs were obtained as a dry powder.

2.4. Preparation of Chitosan (CS) with f-MWCNTs

The preparation of chitosan and multiwalled carbon nanotubes was adapted from Diaconu et al. [38] with some modifications. First, 2 mg of f-MWCNTs were dissolved in 1% CS, which was prepared by dissolving 1 mL chitosan in 1% acetic acid in distilled water. The resulting mixture was stirred for 3 h and then homogenized for 10 min using an ultrasonicator. The mixture was kept at a laboratory temperature of 21.0 ± 2.0 °C and was ready to be used in experiments.

2.5. Pre-Treatment and Preparation of Modified AuE

The bare AuE pre-treatment was conducted using the method previously described by Siddiquee et al. [39]. Next, the AuE was cleaned and rinsed thoroughly with distilled water, and nitrogen gas was used to dry the electrode. Subsequently, 5 μ L of modification materials (f-MWCNTs/CS) were dropped onto the AuE surface (3 mm in diameter) and left to incubate for 2 h. After 2 h, the AuE surface was dried, and the f-MWCNTs/CS were immobilized onto the AuE surface. Then, 10 μ L of Prussian blue was applied to the surface of the modified AuE for 2 min. Following this, a three-electrode system was used to measure current signals over a potential range of 0.0 V to 1.7 V.

2.6. Sensing Mechanism

Figure 1 shows a schematic for the synthesis of CS with f-MWCNTs and its mechanism towards Al^{3+} via electrolysis. Aluminum sulphate, $Al_2(SO_4)_3$, in the solution suggested lysis process breakdown. Aluminum ions (Al^{3+}), the product of a method which generates an electroactive species, can be analyzed using the current signals of electrochemical methods. There are three possible factor interactions between MWCNTs/CS and the target

ion: delocalization of the π - π bond (distribution of electron density) [40], intermolecular hydrogen bond, and intermolecular force [36].

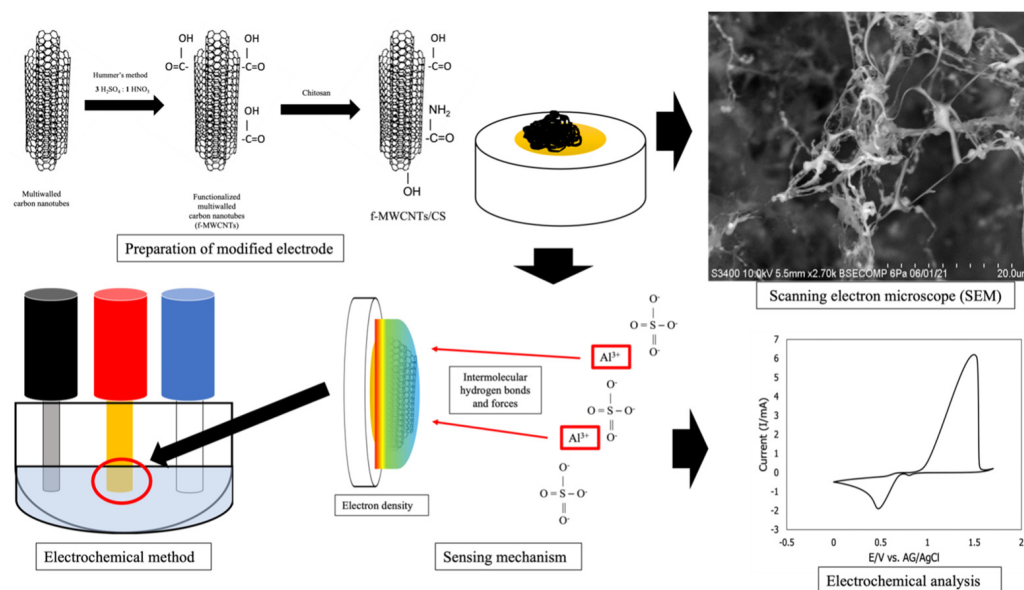


Figure 1. Schematic diagram for the preparation of CS with f-MWCNTs and its mechanism for detection of Al^{3+} using three three-system electrodes (platinum as the counter electrode, gold electrode as the working electrode, and silver/silver chloride as the reference electrode).

3. Results and Discussion

3.1. Physical Morphological Characterization of Nanomaterials

The f-MWCNTs and CS were synthesized and examined with scanning electron microscopy (SEM) (Figure 2A) and transmission electron microscopy (TEM) (Figure 2B). SEM utilizes electron beams to magnify the surface texture of the sample. When electrons are powerfully injected into the sample, the electrons within the sample become unstable and emit. These emitted electrons are translated into electrical signals, which are then displayed as images of the sample's texture. In this experiment, SEM observation (20 μm in diameter) revealed that the network structure of f-MWCNTs/CS had a smooth surface texture generated by the coordination of two functional groups, namely the carboxylic group (COOH) of f-MWCNTs and the alkene group ($=\text{CH}_2$) of CS. According to Shalauddin et al. [28], the interaction between functional groups with different charges self-assembles. TEM images of f-MWCNTs/CS at a magnification of 50 nm is displayed in Figure 2B. The homogenized f-MWCNTs and CS formed well-regarded pipe bundles within this range, as reported by Zhao et al. [29]. The same author noted that the electron transfer rate increased as a result of a larger surface-active area within the same physical observation structure. To better understand the advantages of nanomaterials, further research was performed on the elemental compositions and abundance of f-MWCNTs/CS using energy-dispersive X-ray (EDX) (Figure 2C). According to Table 1, the main element detected was carbon, indicating that nanomaterial synthesis was successful. In addition, our research demonstrated that f-MWCNTs/CS are made of the following components in decreasing order: oxygen > potassium > aluminum > calcium > indium > manganese. To examine the interaction of synthesized f-MWCNTs/CS with target ions (aluminum ions, Al^{3+}), an electrochemical method was used. In this experiment, three variations of the electrode surface were prepared, including a bare gold electrode (AuE), an AuE with Prussian blue (PB) as a redox indicator (PB/AuE), and a modified AuE (f-MWCNTs/CS/PB/AuE). In order to determine the varying responses of nanomaterials in the presence of Al^{3+} under different potentials, PB was deployed. The control of this experiment was electrolytic solution (PBS) without Al^{3+} . This proposedly prepared to distinguish the present signal of

Al^{3+} with other foreign components. The current signals were compared and are shown in Figure 2D. The f-MWCNTs could increase the current signals due to large number of delocalized π electrons by SP^2 hybridization of carbon atoms located at the walls of f-MWCNTs. These electrons increase the conductivity by forming of covalent bond with the π electrons from the polymers [40]. Yet, without CS, f-MWCNTs easily fall off the AuE surface [41]. CS is proposed to be created to maintain f-MWCNTs on the surface, as CS has been reported to be biocompatible and increase electrode conductivity [40]. The highest cyclic voltammetry (CV) current signals were observed in the presence of Al^{3+} for f-MWCNTs/CS/PB/AuE compared to AuE and PB/AuE. The signal was five times stronger for f-MWCNTs/CS/PB/AuE compared to AuE alone. Similar to the findings of Diaconu et al. [38], the current intensity of MWCNT-CS was twice that of a bare gold electrode, indicating a larger electroactive area. We also expect that f-MWCNTs/CS/PB/AuE resulted in a larger surface area for Al^{3+} accumulation. Moreover, the presence of PB played a significant role in shifting the current signals of f-MWCNTs/CS/PB/AuE to a specific potential during redox reactions. Further investigation of the electrochemical behavior of f-MWCNTs/CS/PB/AuE was conducted in the presence of Al^{3+} .

Table 1. Elemental compositions of f-MWCNTs/CS.

Element	Series (wt. %)	unn. (wt. %)	C norm. (at. %)	C atom	(1 Sigma)
Carbon	K-series	48.24	46.35	58.98	5.53
Oxygen	K-series	37.92	36.44	34.81	4.55
Aluminum	K-series	4.58	4.40	2.49	0.24
Potassium	K-series	5.97	5.73	2.24	0.24
Calcium	K-series	1.94	1.86	0.71	0.11
Manganese	K-series	0.53	0.51	0.14	0.08
Indium	L-series	4.91	4.71	0.63	0.21
	Total:	104.08	100.00	100.00	

3.2. Optimization of Parameters

The procedure's parameters were optimized based on our previous work with some modifications [37]. The potential range was set to 0.0–1.7 V, with a scan rate of 0.1 Vs^{-1} and an accumulation time of 15 s in 10 mL of buffer solution (0.1 M, pH 2) containing 0.2 ppm of aluminum. On the modified electrode (f-MWCNTs/CS/PB/AuE), 5 mM of Prussian blue was added.

3.2.1. Effect of Buffer

The CV method was used to test the effectiveness of five different buffers, including acetate buffer, phosphate-buffered saline (PBS), citrate buffer, ammonium buffer, and Tris-HCl buffer, in the presence of aluminum. A f-MWCNTs/CS/PB/AuE was submerged in 10 mL of each respective buffer solution (0.1 M, pH 2). As shown in Figure 3, the current signals obtained from the oxidation and reduction reactions indicated the presence of Al^{3+} in each buffer. Among the buffers tested, PBS displayed the highest current signal during the oxidation reaction, followed by citrate buffer, Tris-HCl buffer, acetate buffer, and ammonium buffer. In contrast, PBS maintained the highest current signal during the reduction reaction compared to other buffers. These findings highlighted the potential for nanomaterials and buffers to be used in tandem for ion detection. Moreover, oxidation catalytic current demonstrated that the electron transfer reaction at the electrode changed with the pH of the buffer solution [36]. In this experiment, the acidity of the buffer had no effect on the structure and function of f-MWCNTs and CS, but it enhanced their electrical conductivity and adhesion strength [20]. Hence, PBS's current signals were the highest among the buffers. However, our previous research revealed that the tris-HCl buffer containing AuE alone produced the maximum signal for detecting Al^{3+} [37]. This is due to the aluminum atom on the surface of the electrode releasing three electrons ($\text{Al} \rightarrow \text{Al}^{3+} + 3\text{e}^-$) and accumulating on the surface-active area of

f-MWCNTs/CS on modified AuE under PBS conditions. It is an interesting finding that PBS provided MWCNTs/CS with good electrical conductivity and a high mass electron transfer. Hence, PBS was applied for the next experiment.

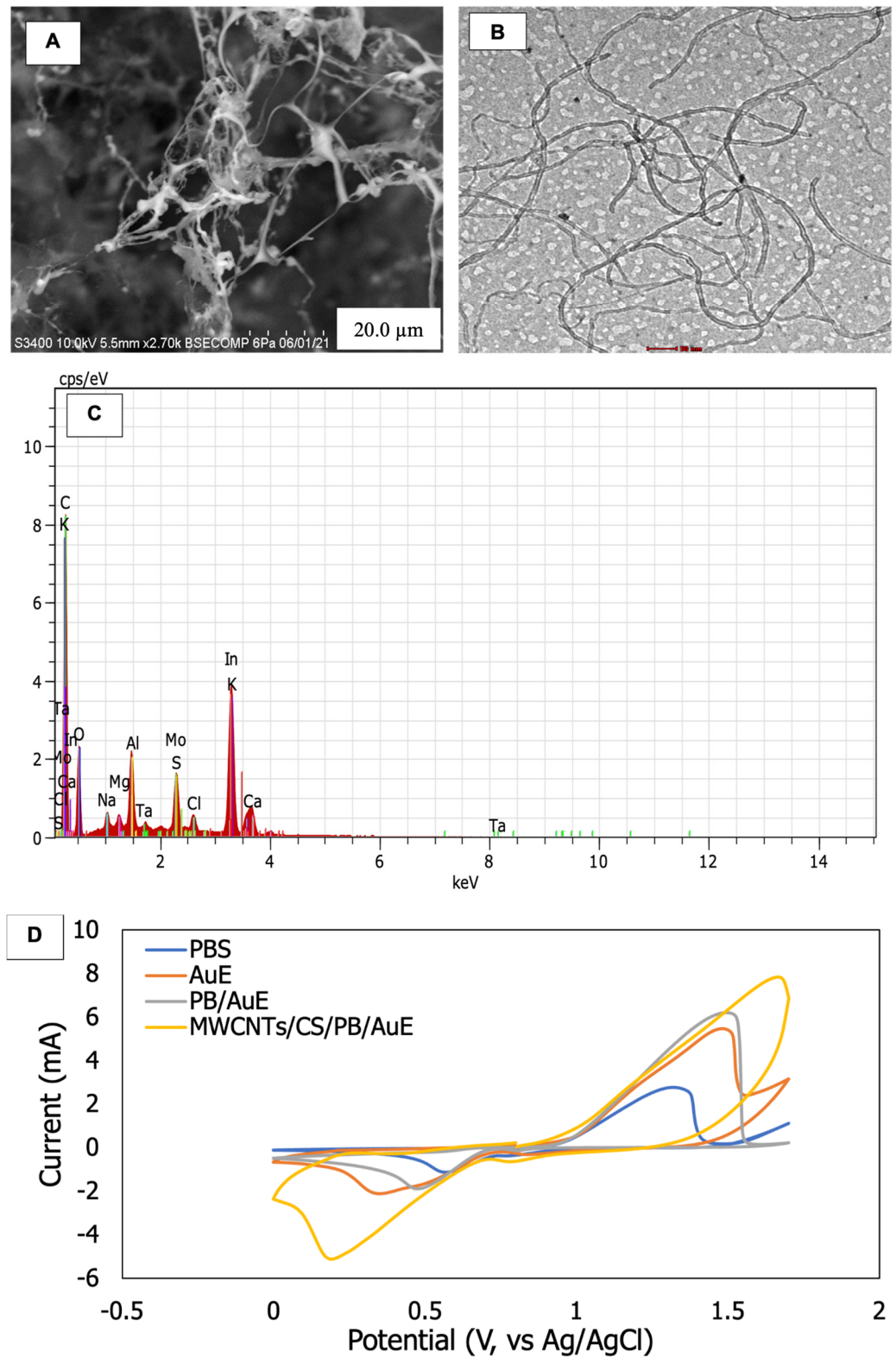


Figure 2. (A) SEM and (B) TEM images observed under different magnifications, (C) EDX analysis of f-MWCNTs, and (D) voltammogram of modified electrodes ($n = 3$).

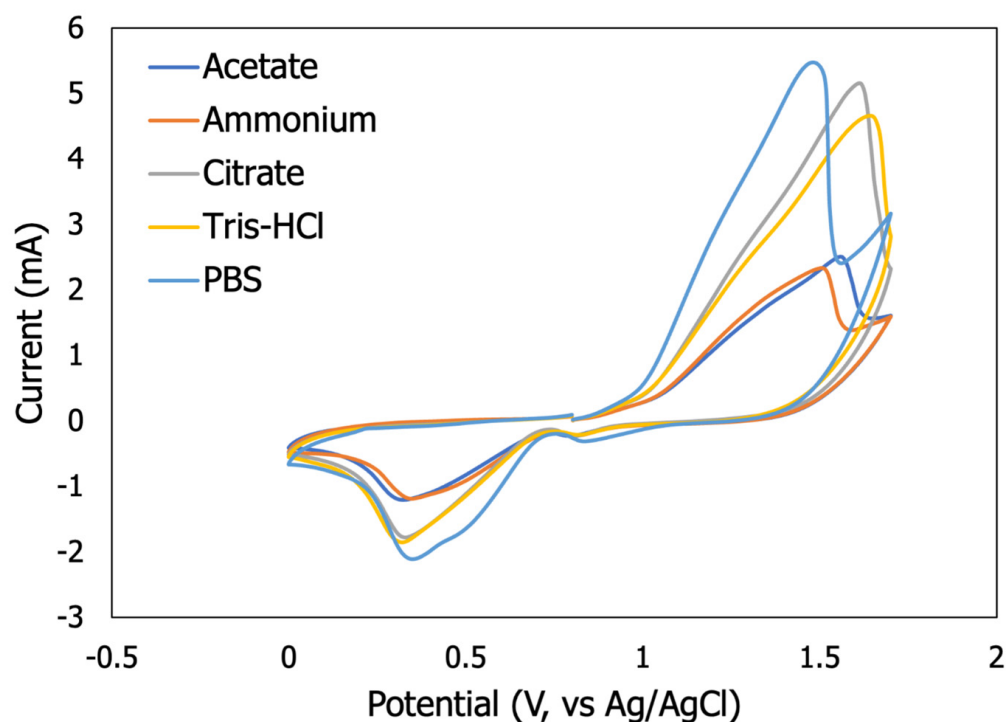


Figure 3. Cyclic voltammograms of different buffers (acetate, ammonium, citrate, Tris-HCl, and PBS) in the presence of 0.2 ppm Al^{3+} tested using f-MWCNTs/CS/PB/AuE. The experimental conditions included a scan rate of 0.1 V s^{-1} and 15 s of accumulation time ($n = 3$).

3.2.2. Effect of pH

The effect of buffer pH on the formation of oxidation and reduction signals of f-MWCNTs/CS/PB/AuE was investigated in the presence of Al^{3+} across a range of pH values from 2 to 9, with intervals of 1. The pH levels and types of the buffer solution were found to have an impact on the signals observed (Figure 4). According to the trend of the peak signals, pH 2 (a) generated the highest peak, which gradually decreased as pH increased. This event was the result of aluminum ions forming hydroxyl complexes [42–44]. $\text{Al}(\text{OH})_3$, aluminum hydroxide, was determined as the compound's species based on the current signals [19]. This compound's insolubility in water interrupted the current signals by depositing on the modified electrode's surface [45]. Previously, the selection of pH buffers focused mostly on acidic conditions [19,42,45]. This is because the absorption rate is affected by electrostatic, repulsive, and dispersive forces. According to Kyriakopoulos et al. [46], as ionic strength rose, the adsorption increased from pH 6.5 to pH 3. As a result of decreased repulsive interactions between solvent and target ions, a low pH value is associated with a high adsorption rate. In the experiment, pH 2 was shown to have the lowest repulsive forces and the highest current signals compared to other pH values. Based on the findings of Arancibia and Muñoz [47], the acidic pH level was also favored for detecting carbon-free (monomeric) inorganic compounds, such as aluminum species. Consequently, pH 2 was chosen as the optimal pH condition based on the present signal, and acidic conditions were supported by the majority of prior researchers.

3.2.3. Effect of Scan Rate

The effect of scan rate on the current signals of f-MWCNTs/CS/PB/AuE in (0.1 M, pH 2) PBS solution in the presence of Al^{3+} was investigated by varying the scan rate from 0.05 to 0.30 V s^{-1} . The results showed a direct proportionality between the scan rate and the current signals, with the current signals increasing from 0.05 to 0.25 V s^{-1} until unstable signals were produced. When the scan rate exceeded 0.25 V s^{-1} , the stability of the current decreased at the oxidation signal of 0.30 V s^{-1} , leading to an asymmetrical

CV curve, as depicted in Figure 5A. The generation of unstable current signals due to the “noise” of the current is a well-known phenomenon called overvoltage or potential overcurrent, which occurs at high current transfer rates. Figure 5B shows the plot of the oxidation peak (I_{pa}) and reduction peak (I_{pc}) from 0.05 to 0.25 Vs^{-1} . The linearity of I_{pa} and I_{pc} were determined by f-MWCNTs/CS/PB/AuE, with $y = 1.0892x + 3.2044$, $R^2 = 0.9828$ for I_{pa} , and $y = 0.9455x + 0.0902$, $R^2 = 0.9767$ for I_{pc} . Based on the stability of the current signal and the highest peak signal generated during the experiment, a scan rate of 0.25 Vs^{-1} was selected.

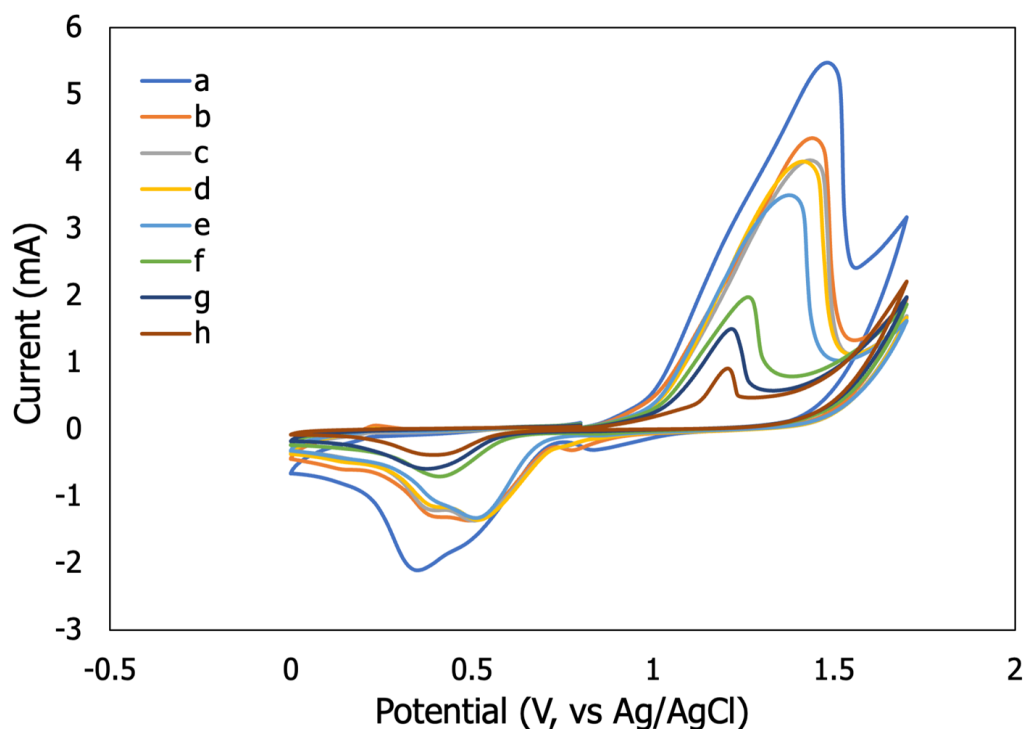


Figure 4. Cyclic voltammograms of f-MWCNTs/CS/PB/AuE recorded at different pH values ranging from pH 2 to pH 9 (in intervals of 1) (a to h) in the presence of 0.2 ppm Al^{3+} . The experimental conditions included the use of 0.1 M PBS as the supporting electrolyte solution with a scan rate of 0.1 Vs^{-1} and an accumulation time of 15 s ($n = 3$).

3.2.4. Effect of Accumulation Time

The effect of duration on the detection of Al^{3+} by f-MWCNTs/CS/PB/AuE in electrolytic solution (0.1 M, pH 2 of PBS) was evaluated over a range of 5 to 40 s (in 5 s intervals). The system was generating current before the signal readings were taken, indicating that it had already stabilized. The results showed that the formation of the current signal increased from 5 to 25 s and then decreased at 40 s (Figure 6). This behavior is likely due to the memory effect of the modified AuE surface, which is highly tolerant of Al^{3+} concentrations. A high concentration of Al^{3+} may have prevented other ions from attaching to the surface [19]. Thus, the optimal accumulation time for detecting Al^{3+} was determined to be 25 s.

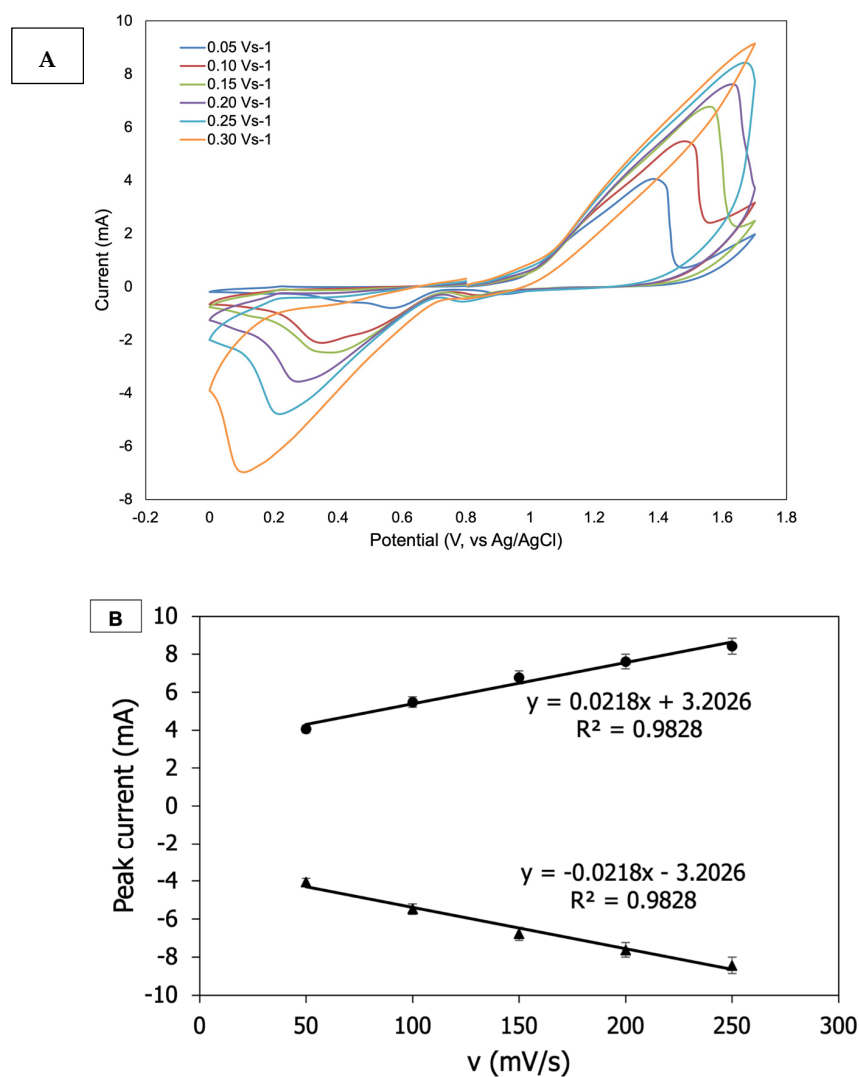


Figure 5. (A) Cyclic voltammograms obtained at different scan rates on f-MWCNTs/CS/PB/AuE in the presence of 0.2 ppm Al³⁺. The scan rates ranged from 0.05 to 0.30 Vs⁻¹. The experimental conditions included 0.1 M PBS as the supporting electrolyte and 15 s of accumulation time ($n = 3$). (B) Peak values of the oxidation and reduction signals measured and plotted against the corresponding scan rates.

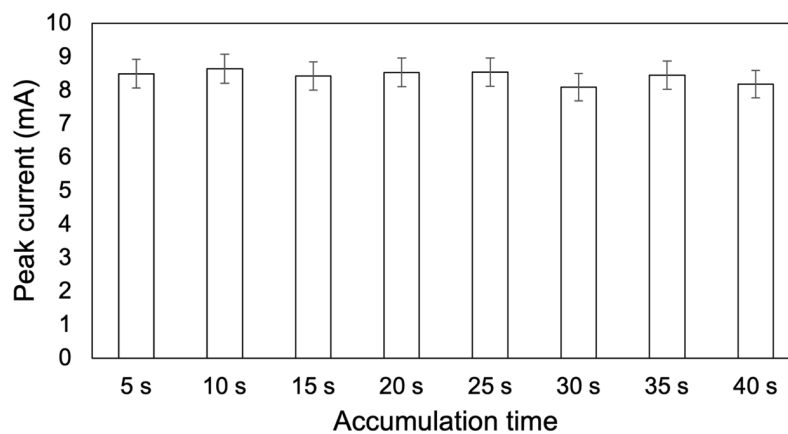


Figure 6. Bar graph of the effect of different accumulation times on the current signal of f-MWCNTs/CS/PB/AuE in the presence of 0.2 ppm Al³⁺. The experimental conditions included 0.1 M PBS as the supporting electrolyte and a scan rate of 0.25 Vs⁻¹ ($n = 3$).

3.2.5. Effect of Volume

To investigate the effect of the target ion concentration in buffer solution, a mixture of 10 mL buffer (0.1 M, pH 2) and sample solution was prepared using volume ratios (v/v) of 8 mL:2 mL, 6 mL:4 mL, 4 mL:6 mL, and 2 mL:8 mL, respectively, as calculated with modifications according to Chaiyo et al. [48]. Figure 7 illustrates the impact of volume ratio on the performance of f-MWCNTs/CS/PB/AuE in detecting Al^{3+} . The results showed that the current signal of volume ratio b (4:6) was higher than that of the other volume ratios, suggesting that the volume ratio influenced the formation of the current signal. Thus, the volume ratio of 4:6 mL was selected for the analysis of the sample. Hence, 4 mL of analyte volume and 6 mL of buffer volume were determined to be the optimal ratio for detecting Al^{3+} with the highest analytical performance.

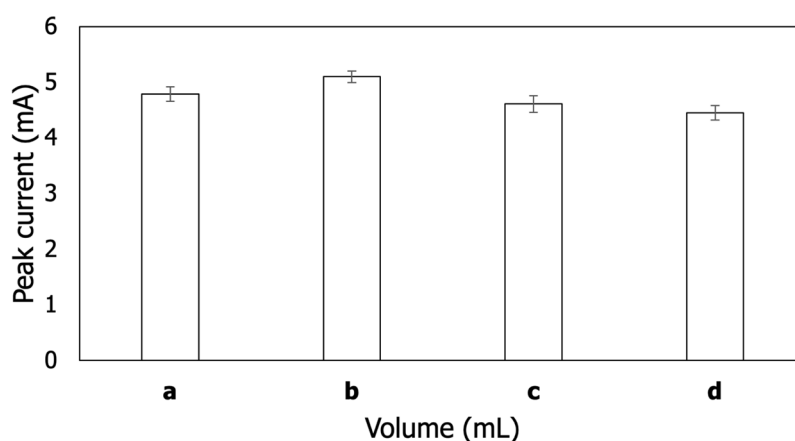


Figure 7. Cyclic voltammogram of different analytical volumes on f-MWCNTs/CS/PB/AuE in the presence of Al^{3+} ; (a) 2 mL of analyte and 8 mL of buffer, (b) 4 mL of analyte and 6 mL of buffer, (c) 6 mL of analyte and 4 mL of buffer, and (d) 8 mL of analyte and 2 mL of buffer. The experimental conditions were 0.1 M PBS as a supporting electrolyte under a 0.25 Vs^{-1} scan rate for 25 s of accumulation time ($n = 3$).

3.3. Analytical Performance

3.3.1. Surface Active Area

We re-evaluated the current signals of bare AuE, PB/AuE, and f-MWCNTs/CS/PB using the optimal parameters obtained from the optimization experiment. In agreement with Figure 8, f-MWCNTs/CS/PB/AuE exhibited the highest oxidation current signal of 7.69 mA, while the reduction current signal was -5.10 mA . These results suggest that the modified electrode has the potential to detect the presence of Al^{3+} by creating a specific active area and enhancing electron kinetic transfer under optimal conditions. To determine the active area of the electrodes, we used the formula for surface active area performed by Lee et al. [49] based on the Randles–Sevcik equation [50]:

$$i_p = 2.69 \times 10^5 n A C_0 D^{1/2} \nu^{1/2} \quad (1)$$

To measure the surface-active area (A), Equation (1) derived to form Equation (2) and it expressed as

$$A = i_p / 2.69 \times 10^5 n C_0 D^{1/2} \nu^{1/2} \quad (2)$$

The i_p is peak current, n is the number of electron transfer, C_0 is the bulk concentration of redox, D is diffusion coefficient and ν is the scan rate. In this experiment, a 5 mM Prussian blue undergoes one-electron transfer ($n = 1$) on the electrode surface with A representing the surface-active area, C_0 the bulk concentration of redox (0.005 M), $D = 6.67 \times 10^{-6}$ the diffusion coefficient, and ν the scan rate (0.25 Vs^{-1}). The surface-active areas of the electrodes after optimization experiments are listed in Table 2. Based on the table, the widest specific surface areas for both oxidation and reduction signals were observed with

f-MWCNTs/CS/PB/AuE, measuring 6.86 cm² and 4.55 cm², respectively. These findings demonstrate the advantages of using nanomaterials to provide a specific target area for the ion being detected.

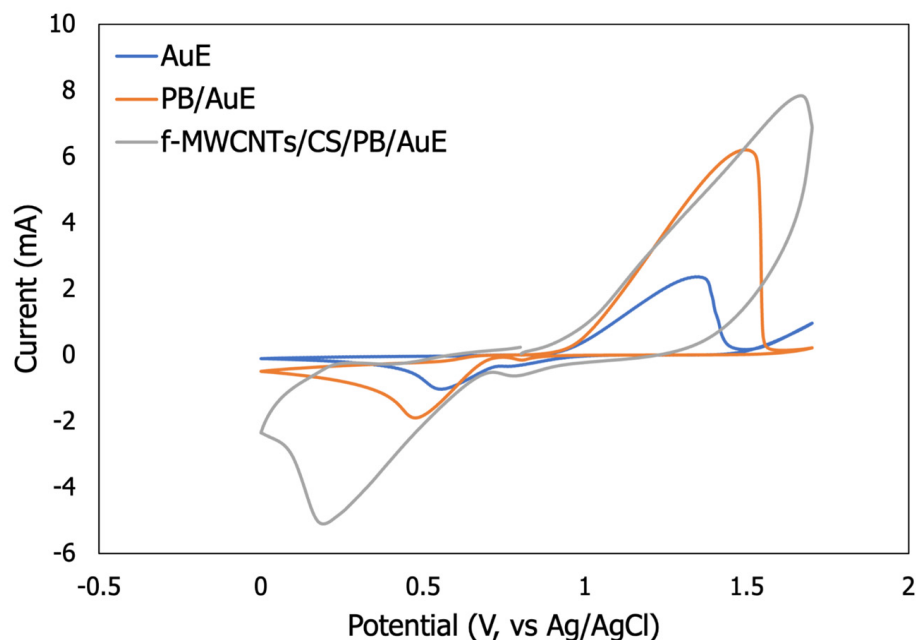


Figure 8. Cyclic voltammograms of various modified electrodes in the presence of Al³⁺ under the following experimental conditions: 10 mL of (0.1 M, pH 2) PBS served as the supporting electrolyte with a scan rate of 0.25 Vs⁻¹ and an accumulation time of 25 s ($n = 3$).

Table 2. The current signal and surface-active area of the electrodes.

Electrode Configuration	I _{pa} (mA)	Surface Active Area (cm ²)	I _{pc} (mA)	Surface Active Area (cm ²)
AuE	2.36	2.10	-1.03	0.91
PB/AuE	6.19	5.52	-1.89	1.69
f-MWCNTs/CS/PB/AuE	7.69	6.86	-4.55	4.55

3.3.2. Repeatability and Reproducibility

To evaluate the repeatability, five-cycle readings of f-MWCNTs/CS/PB/AuE were taken under the same conditions, and the peak with the greatest height among the five signals was plotted and compared. As shown in Figure 9A, the peaks decreased as the number of cycles increased, indicating that the modified electrode generated unsteady current signals and could not be used repeatedly. Next, a reproducibility test was conducted using five different preparations of f-MWCNTs/CS/PB/AuE. Figure 9B shows the current readings for the reproducibility test of five identically produced current signals. These results demonstrated that the modified electrode can be used with various samples without compromising the sensor's stability. Based on $n = 5$, we computed the relative standard deviation (RSD) of repeatability and reproducibility (five readings for each current formation on their slopes). As shown in Table 3, the RSDs for repeatability and reproducibility were 0.58% and 5.2%, respectively, indicating that f-MWCNTs/CS/PB/AuE has a high degree of stability for detecting Al³⁺ in various samples.

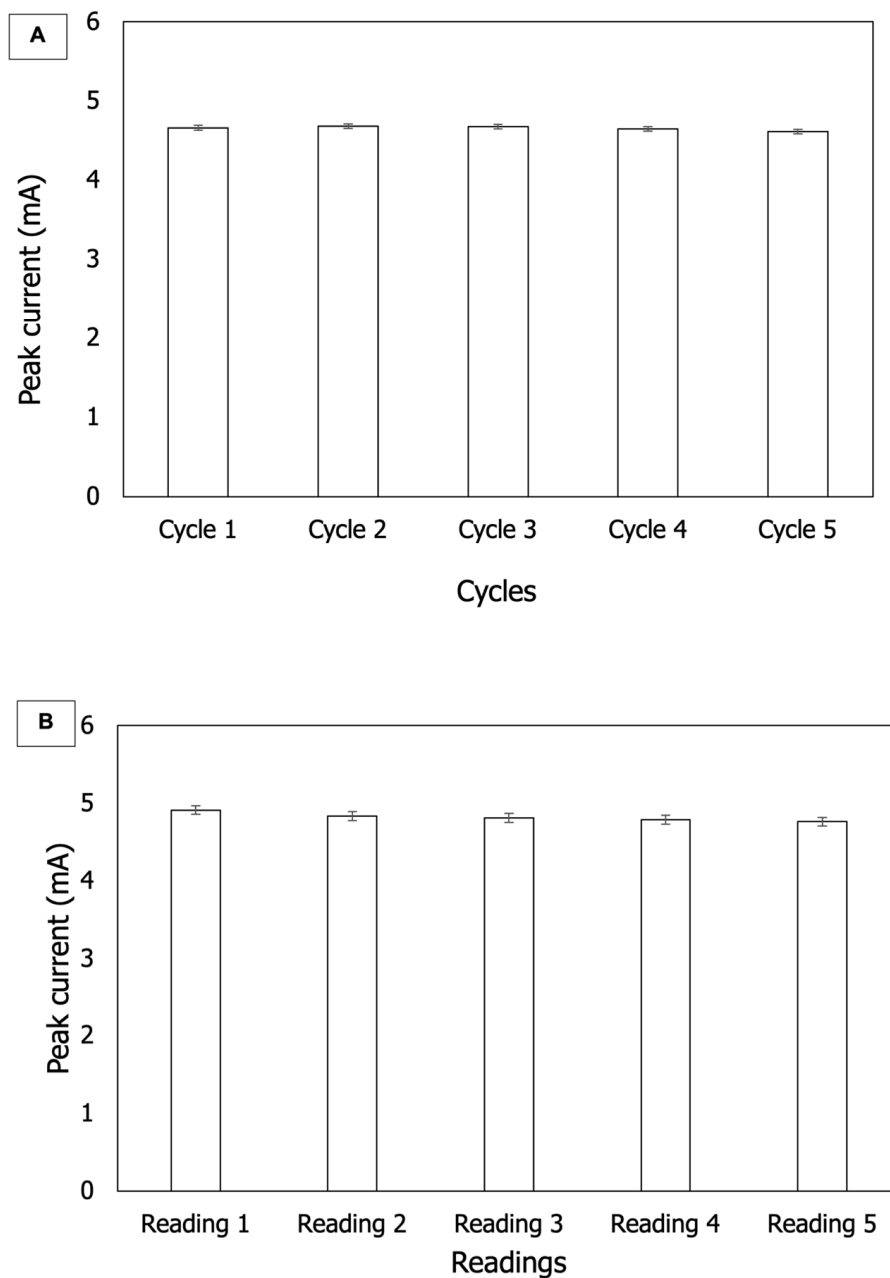


Figure 9. Bar charts of (A) repeatability and (B) reproducibility tests on f-MWCNTs/CS/PB/AuE in the presence of Al^{3+} ($n = 5$).

Table 3. RSD of repeatability and reproducibility.

Characteristic	Mean \pm STD	RSD (%)
Repeatability	4.56 \pm 0.02	0.58
Reproducibility	4.75 \pm 0.24	5.20

3.3.3. Interfering Study

In this experiment, MnSO_4 , CaCO_3 , CuSO_4 , FeSO_4 , ZnSO_4 , K_2SO_4 , and Na_2CO_3 were used to generate Mn^{2+} , Ca^{2+} , Cu^{2+} , Fe^{2+} , Mg^{2+} , Zn^{2+} , K^+ , and Na^+ ions, respectively. The effect of each interfering ion on the target ion was individually examined by adding 0.2 ppm of the interfering ion to an electroanalytical solution containing the same amount of Al^{3+} [49]. The current signals of the eight interfering ions in the presence of Al^{3+} are

presented in Figure 10. As the peak current signals of Al^{3+} were the highest among the metal ions tested, the results indicate that no significant interference (p -value of 0.0) was observed. Moreover, potential interfering ions such as Zn^{2+} , Fe^{2+} , and Cu^{2+} that could affect the selectivity of current signals were not identified [35,44,47,51]. Therefore, the f-MWCNTs/CS/PB/AuE modified electrode exhibited high selectivity for detecting Al^{3+} in electroanalytical solutions containing other metal ions. The relationship between the target ion and other ions was analyzed using one-way ANOVA, and the results are shown in Table 4. The current signal was found to be dependent on the presence of aluminum, as indicated by the high DPV signal in its presence and the low DPV signal in its absence. This suggests that f-MWCNTs/CS/PB/AuE have a specificity for detecting aluminum. ANOVA tests were performed to determine any differences between the overall groups, while the Tukey Post Hoc test was used to study the differences between the overall groups and a specific group [52]. The results showed that there was no significant interference among the groups, with a p -value of 0.0 obtained.

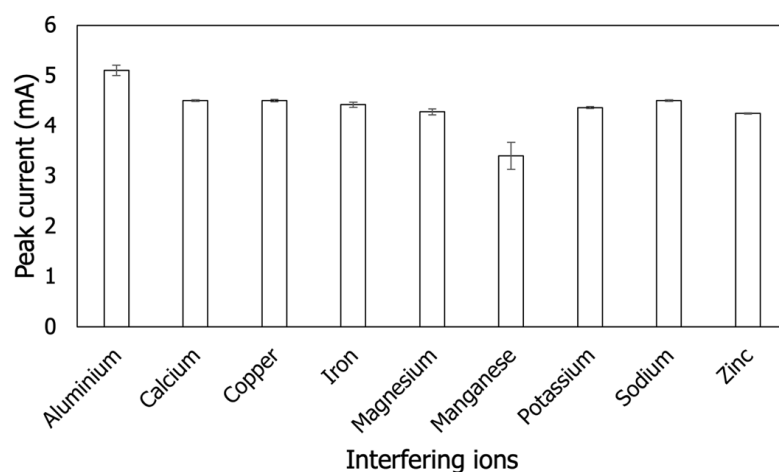


Figure 10. Bar chart of different interferer ions in the presence of Al^{3+} on modified electrode (f-MWCNTs/CS/PB/AuE) ($n = 3$).

Table 4. One-way ANOVA analysis of aluminium ion in the presence of interfering ions.

ANOVA				
	Sum of Squares	Current df	Mean Square	F
Between Groups	13.226	8	1.653	90.823
Within Groups	1.213	18	0.067	
Total	14.438	26		
Post Hoc Tests				
Target Ion	Interfering Ion	Mean Difference	Significant value	
Aluminium	Calcium	0.957	0.00	
	Copper	0.994	0.00	
	Iron	1.039	0.00	
	Magnesium	1.182	0.00	
	Manganese	2.059	0.00	
	Potassium	1.129	0.00	
	Sodium	0.899	0.00	
	Zinc	1.214	0.00	

3.3.4. Storage Stability

Before the experiment was conducted, the modified electrode (f-MWCNTs/CS/PB/AuE) was stored in a dark and dry place, following the method by Ramezani et al. [19]. Differential pulse voltammetry (DPV) was used to measure the current signal, which was indicative of the specific potential generated by the interaction of f-MWCNTs/CS/PB/AuE with varying current intensities towards Al^{3+} . The results showed that the current intensities decreased as the modified electrode was stored for a longer period of time (Figure 11). The variation in current signal from the first day to the seventh day was 4.20%, whereas the variation beyond seven days was 14.01% and 53.48%, respectively. After more than two weeks, the performance of the modified electrode could degrade.

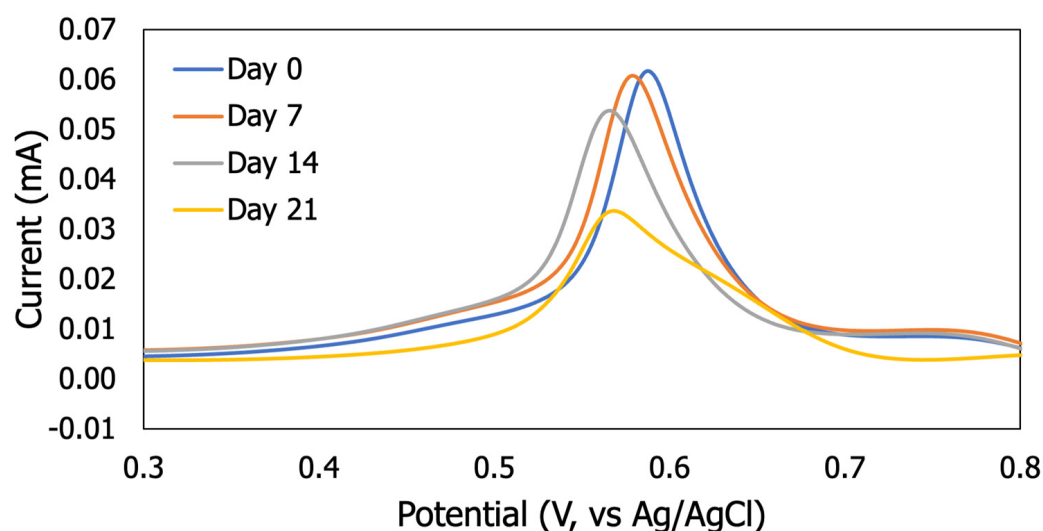


Figure 11. Effect of the storage stability test on modified electrode (f-MWCNTs/CS/PB/AuE) for every week of the current measurement until the third week ($n = 3$).

3.3.5. Concentration Analysis

The various concentrations of Al^{3+} ranging from 0.0 ppm to 3 ppm were tested using the DPV method (Figure 12A). The results showed that the current signals of f-MWCNTs/CS/PB/AuE increased with increasing concentrations of Al^{3+} . This phenomenon suggested that the modified electrode provided a large surface area for Al^{3+} to occupy. The linearity of f-MWCNTs/CS/PB/AuE with varying concentrations of Al^{3+} is shown in Figure 12B, where the linearity from 0 to 1 ppm was $y = 0.0387x + 0.0748$ with a high correlation coefficient of $R^2 = 0.9853$. A recent study by Geng et al. [40] reported the detection of chloramphenicol using a modified chitosan-multiwall carbon nanotubes (CS-MWCNTs) and molecularly imprinted polymers (MIPs) on glassy carbon electrode (GCE) with good linearity ($R^2 = 0.9893$). Table 5 summarizes the various applications of modified chitosan-multiwalled carbon nanotubes for detecting different materials and sources. In this experiment, the LOD, LOQ and sensitivity of f-MWCNTs/CS/PB/AuE were determined as 0.002 ppm, 0.007 ppm, and $0.0865 \text{ ppm}^{-1} \text{ cm}^{-2}$, respectively [53]. The LOD of this modified electrode was compared to the previous detections listed in Table 6, indicating that it provided the latest information for detecting Al^{3+} in drinking water.

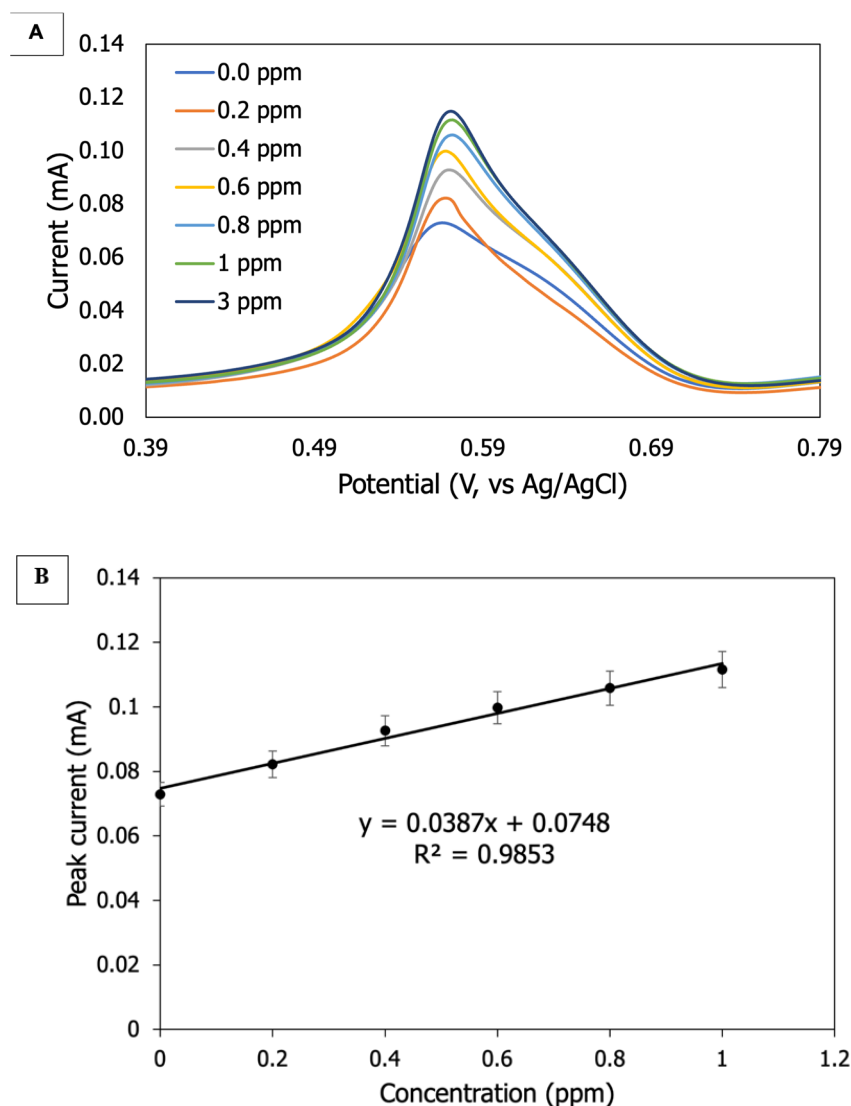


Figure 12. Effect of different concentrations of Al^{3+} on modified electrode (f-MWCNTs/CS/PB/AuE): (A) DPV analysis and (B) formation of peak signals ($n = 3$).

Table 5. The application of chitosan-multiwalled carbon nanotubes with some modifications, linearity (R^2), linear of range (LOR), and limit of detection (LOD) for detecting specific targets.

References	Target	Modification	Correlation Coefficient, R^2	LOR	LOD
This work	Aluminum	Functionalized multiwalled carbon nanotubes/chitosan/Prussian blue/gold electrode (f-MWCNTs/CS/PB/AuE)	0.9853	0.0–1 ppm	5.84×10^{-9} mol/L (0.002 ppm)
[20]	Diethylstilbestrol	Gold nanoparticles/multi-walled carbon nanotubes-chitosan/glassy carbon electrode (AuNPs/MWCNTs-CS/GCS)	0.9996	1.0×10^{-10} – 1.0×10^{-6} mg/mL	24.3 fg/mL
[23]	Acetylcholine	Chitosan-multi-walled carbon nanotubes-iron (II, III) oxide nanoparticles/AChE-ChO/glassy carbon electrode (CS-MWCNTs- Fe_3O_4 NPs/AChE-ChOx/GCE)	0.993 and 0.989	0.02–0.111 μ mol/L and 0.111–1.87 μ mol/L	0.61 nmol/L and 0.002 μ mol/L

Table 5. Cont.

References	Target	Modification	Correlation Coefficient, R ²	LOR	LOD
[24]	Zearalenone	Chitosan functionalized acetylene black and multi-walled carbon nanotubes/glassy carbon electrode (CS@AB-MWCNTs/GCE) Multilayer core-shell type superparamagnetic and water-compatible/ multi-walled carbon	0.9939	10.0 fg–1.0 ng m/L	3.64 fg m/L
[29]	Diethylstilbestrol	nanotubes@chitosan/surfactant hexadecyl trimethyl ammonium bromide/magnetic glassy carbon electrode (WMMIPs/MWCNTs@CS/CTABr/MGCE)	0.9989	1.2×10^{-8} – 1.5×10^{-4} mol/L	4.5×10^{-9} mol/L
[30]	Vanillin and tartrazine	Copper(II) sulfide@ carboxylated carbon nanotubes/glassy carbon electrode (CuS@COOH-MWCNTs/GCE)	0.9929 and 0.9935	0.03–125 μ M	0.006 μ M and 0.005 μ M
[31]	Tryptophan	Chitosan/Ce-MOF/glassy carbon electrode (Cs/Ce-MOF/GCE)	0.995	0.25–331 μ M	0.14 μ M
[36]	Glucose	Flavin adenine dinucleotide (FAD)-glucose dehydrogenase/ chitosan-multiwalled carbon nanotubes/ screen-printed carbon electrodes (GDH/CS-MWCNT-5/ SPCEs)	0.99646	0–5.5 mM	0.01563 mM
[38]	Phenolic acids	Laccase-multiwall carbon nanotubes (MWCNT)–chitosan (CS)/gold sheets (Lacc–CS–MWCNT/Au)	0.9968	7.35×10^{-7} – 1.05×10^{-5} mol/L	1.51×10^{-7} mol/L
[40]	Chloramphenicol	Chitosan-multiwalled carbon nanotubes/molecularly imprinted polymers/glassy carbon electrode (CS-MWCNTs/MIPs/GCE)	0.9893	0.1–1000 ng/mL	3.3×10^{-2} ng/mL
[41]	Indole	Multiwalled carbon nanotubes–chitosan/ screen-printed carbon electrode (MWCNTs-CS/SPCE)	0.9905	5–100 μ g/L	0.5 μ g/L
[54]	Staphylococcus aureus gene sequence	Single-stranded DNA/gold nanoparticles/ chitosan-multiwalled carbon nanotubes/gold electrode (ssDNA/Au-NPs/CS–MWCNTs/AuE)	0.9945	1.0×10^{-15} to 1.0×10^{-8} M	3.3×10^{-16} M
[55]	Epinephrine and uric acid	Gold nanoparticles/thioglycolic acid film/ chitosan-multiwalled carbon nanotubes/glassy carbon electrode (AuNPs/TGA/CS–MWCNTs/GCE)	0.9924 and 0.9912	0.7–7 μ M and 7–133 μ M	85 nM and 45 nM
[56]	Acetaminophen and p-aminophenol	1,3,5-tris-(4-formylphenyl) benzene-benzidine- covalent organic framework/caCTF-1–700/carboxylated carbon nanotubes/glassy carbon electrode (TFPB-BD-COF/caCTF-1–700/COOH-MWCNT/GCE)	0.9940 and 0.9980	0.6–150 μ M	0.053 μ M and 0.075 μ M
[57]	Hydrogen peroxide	Copper nanoparticles/methylene blue/ multiwall carbon nanotubes–fullerene–chitosan–ionic liquid/glassy carbon electrode (CuNPs/MB/MWCNT-C ₆₀ -Cs-IL/GCE)	0.9906	0.2 μ M–2.0 mM	55.0 nM
[58]	Lysozyme	Reduced graphene oxide–multi-walled carbon nanotubes/ chitosan/ synthesized carbon quantum dot/glassy carbon electrode (rGO-MWCNT/CS/ CQD/GCE)	0.9985 and 0.9987	20–10 nmol/L and 10–100 nmol/L	3.7 and 1.9 fmol/L

Table 6. The comparison of the modifications used for determining Al³⁺ based on previous reports.

References	Real Samples	Modification	LOD (mol L ⁻¹)
This work	Drinking water	Multiwalled carbon nanotubes/chitosan/Prussian Blue/gold electrode (f-MWCNTs/CS/PB/AuE)	5.84 × 10 ⁻⁹ (0.001 ppm)
[7]	Green tea, river and tap water	Schiff base/screen printed electrode (JS1/SPE)	2.26 × 10 ⁻⁹
[18]	Drinking water	Gold nanoparticles@tannic acid/glassy carbon electrode (AuNPs@TA-GCE)	10.0 × 10 ⁻⁹
[19]	Mineral water, Al-Mg syrup, black tea extract and ore samples	Nano-Cs-polyoxomolybdate/ionic liquid/carbon paste electrode (Nano-PMo12/IL/CPE)	7.94 × 10 ⁻¹⁰
[35]	Waste and river water	Alizarin S-Al complex	7.41 × 10 ⁻⁵
[42]	Alloy, drugs, and food products	AlMCM-41/modified carbon paste electrode (AlMCM-41/MCPE)	4.6 × 10 ⁻⁷
[43]	Tea leaves and Al-Mg samples	Sol-gel-Au nanoparticle/2,2'-dihydroxy-1-naphthylidene-1'-naphthyl methyl amine/carbon paste electrode (SGAN/DNMA/CPE)	2.0 × 10 ⁻¹⁰
[44]	Rock samples	7-Ethylthio-4-oxa-3-phenyl-2-thioxa-1,2-dihydropyrimido-[4,5-d]pyrimidine/ <i>o</i> -nitrophenyloctyl ether/poly (vinyl chloride) (ETPTP/ <i>o</i> -NPOE/PVC)	1.8 × 10 ⁻⁵
[45]	Foods and water	Cupferron/hanging mercury drop electrode (Cupferron/HMDE)	2.96 × 10 ⁻⁸
[47]	Sea water	Aluminium (pyrogallol red) x tetrabutylammonium tetrafluoroborate (Al(PR) ₃ x ⁹ TBATFB)	3.7 × 10 ⁻⁵
[59]	Water and metallurgical samples	Cupferron/rotating-disc Cupferron/bismuth film electrode (Cupferron/BiFE)	2.96 × 10 ⁻⁸
[60]	Zinc plating and red mud	Poly(vinyl chloride)/morin/sodium tetraphenyl borate:tri- <i>n</i> -butylphosphate/saturated calomel electrodes	3.2 × 10 ⁻⁷
[61]	River and tap water	Norepinephrine/hanging mercury drop electrode (NE/HMDE)	1.8 × 10 ⁻⁶
[62]	Tea samples	Al(III)-8-hydroxyquinoline/ hanging mercury drop electrode (Al-8HQ/HMDE)	8.54 × 10 ⁻⁸
[63]	Al-Mg syrup and drinking water	Bis(5-phenyl azo salicylaldehyde) naphthalene diamine/polyvinylchloride (5PHAZOSALNPHN/PVC)	2.3–2.5 × 10 ⁻⁶

3.3.6. Accuracy Test

Drinking water samples were collected from local grocery shops in Kota Kinabalu, Sabah, Malaysia. The samples were then individually diluted with 0.2 ppm, 0.6 ppm, and 3 ppm of Al³⁺. The current signals of the diluted samples were compared with those of the control samples (analytical solution). The percent recovery (%R) was calculated based on the peak current signals using the following formula:

$$\text{Percent recovery (\%R)} = (\text{signal of concentration added} / \text{signal of concentration found}) \times 100 \%$$

Based on Table 7, the percent recovery (%R) ranged between 98.66% and 99.66%, while the relative standard deviation (RSD) ranged between 3.55% and 4.6%. This study indicates that the local drinking water is free from Al³⁺ and safe for consumption. Also, the ability of this modified sensor to detect the physical properties of aluminum (it exists

in clear and is invisible in the environment) is highly valued because it enables us to monitor approximately 30 % and 0.61 % of the world's groundwater and surface water drinking water sources, respectively [64,65]. In the experiment, aluminum ions as low as 5.84×10^{-9} M were detected. According to recent findings by Chen et al. [30] in Table 5, the lowest detection levels for MWCNTs and CS are 0.006 M for vanillin and 0.005 M for tartrazine. On the basis of these findings, three distinct targets were found under the same nanomaterials (MWCNTs-CS) with modifications. Therefore, the further understanding of the fundamental of the MWCNTs-CS on specific detection is highly required.

Table 7. The recovery value of Al^{3+} found in drinking water.

Concentration (ppm)	Current Signal of Concentration Added (ppm)	Current Signal of Concentration Found (ppm) Mean \pm Standard Deviation	Recovery (%)	RSD (%)
0.2	8.27×10^{-2}	$8.16 \times 10^{-2} \pm 2.90 \times 10^{-3}$	98.66	3.55
0.6	9.97×10^{-2}	$9.91 \times 10^{-2} \pm 3.46 \times 10^{-3}$	99.39	3.49
3	11.46×10^{-2}	$11.41 \times 10^{-2} \pm 5.32 \times 10^{-3}$	99.56	4.66

4. Conclusions

In this research, the modified electrode has been deployed for specific detection of aluminum ions (Al^{3+}) using application of multiwalled carbon nanotubes and chitosan. The wide surface-active area, good conductivity, great stability, and high selectivity were exhibited by these nanomaterials. The optimal conditions have an effect on the performance of multiwalled carbon nanotubes and chitosan. Moreover, Prussian blue serves as an excellent indicator of specific current potential. Moreover, this method detected Al^{3+} concentrations as low as 5.84×10^{-9} mol/L ($R^2 = 9893$) with an accuracy range of 98.66–99.66%, making it suitable for detecting aluminum in drinking water.

Author Contributions: G.R. and S.S. (Shafiquzzaman Siddiquee) conceived and designed the experiment; G.R. performed the experiment. G.R. and S.S. (Suryani Saallah) analyzed the data; S.S. (Shafiquzzaman Siddiquee), S.S. (Suryani Saallah) and M.T.M.L. provided reagents/materials/analysis tools; G.R. wrote the paper. All authors have read and agreed to the published version of the manuscript.

Funding: This work was supported by UMSgreat (GUG0236-1/2018) of the University Sabah Malaysia.

Institutional Review Board Statement: Not applicable.

Informed Consent Statement: Not applicable.

Data Availability Statement: All data are included in the main text. All data used in the current research are available from the corresponding author on reasonable request.

Acknowledgments: The authors would like to acknowledge the authority of Biotechnology Research Institute (BRI), University Malaysia Sabah (UMS) for providing necessary research facilities. This work was also supported by Borneo Research Marine Institute, Universiti Malaysia Sabah.

Conflicts of Interest: The authors declare no conflict of interest on competing financial interests or personal relationships that could have appeared to influence the work reported in this paper.

References

- Sarkar, D.; Ghosh, P.; Gharami, S.; Mondal, T.K.; Murmu, N. A novel coumarin based molecular switch for the sequential detection of Al^{3+} and F^- : Application in lung cancer live cell imaging and construction of logic gate. *Sens. Actuators B Chem.* **2017**, *242*, 338–346. [[CrossRef](#)]
- Painuli, R.; Joshi, P.; Kumar, D. Cost-effective synthesis of bifunctional silver nanoparticles for simultaneous colorimetric detection of Al (III) and disinfection. *Sens. Actuators B Chem.* **2018**, *272*, 79–90. [[CrossRef](#)]
- Mergu, N.; Singh, A.K.; Gupta, V.K. Highly sensitive and selective colorimetric and off-on fluorescent reversible chemosensors for Al^{3+} based on the rhodamine fluorophore. *Sensors* **2015**, *15*, 9097–9111. [[CrossRef](#)]
- Richardson, S.D. Disinfection by-products and other emerging contaminants in drinking water. *TrAC Trends Anal. Chem.* **2003**, *22*, 666–684. [[CrossRef](#)]

5. Rastogi, L.; Dash, K.; Ballal, A. Selective colorimetric/visual detection of Al^{3+} in ground water using ascorbic acid capped gold nanoparticles. *Sens. Actuators B Chem.* **2017**, *248*, 124–132. [CrossRef]
6. Kim, H.S.; Angupillai, S.; Son, Y.A. A dual chemosensor for both Cu^{2+} and Al^{3+} : A potential Cu^{2+} and Al^{3+} switched YES logic function with an INHIBIT logic gate and a novel solid sensor for detection and extraction of Al^{3+} ions from aqueous solution. *Sens. Actuators B Chem.* **2016**, *222*, 447–458. [CrossRef]
7. Rana, S.; Mittal, S.K.; Singh, N.; Singh, J.; Banks, C.E. Schiff base modified screen printed electrode for selective determination of aluminium (III) at trace level. *Sens. Actuators B Chem.* **2017**, *239*, 17–27. [CrossRef]
8. Ministry of Health Malaysia. National Standard Drinking Water Quality. Engineering Service Division. 2018. Available online: <http://www.gunungganang.com.my/pdf/Malaysian-Policies-Standards-Guidelines/Standards/National%20Drinking%20Water%20Quality%20Standard.pdf> (accessed on 13 March 2023).
9. Egbueri, J.C.; Ameh, P.D.; Unigwe, C.O. Integrating entropy-weighted water quality index and multiple pollution indices towards a better understanding of drinking water quality in Ojoto area, SE Nigeria. *Sci. Afr.* **2020**, *10*, e00644. [CrossRef]
10. Mazhar, S.N.; Ahmad, S. Assessment of water quality pollution indices and distribution of heavy metals in drinking water in Ramganga aquifer, Bareilly District Uttar Pradesh, India. *Groundw. Sustain. Dev.* **2020**, *10*, 100304. [CrossRef]
11. Ling, Y.; Chen, L.X.; Dong, J.X.; Li, N.B.; Luo, H.Q. A simple and rapid method for direct determination of Al (III) based on the enhanced resonance Rayleigh scattering of hemin-functionalized graphene-Al (III) system. *Spectrochim. Acta A Mol. Biomol. Spectrosc.* **2016**, *156*, 22–27. [CrossRef]
12. Hayashi, A.; Sato, F.; Imai, T.; Yoshinaga, J. Daily intake of total and inorganic arsenic, lead, and aluminum of the Japanese: Duplicate diet study. *J. Food Compos. Anal.* **2019**, *77*, 77–83. [CrossRef]
13. Skalny, A.V.; Kaminskaya, G.A.; Krekesheva, T.I.; Abikenova, S.K.; Skal'naya, M.G.; Bykov, A.T.; Tinkov, A.A. Assessment of hair metal levels in aluminium plant workers using scalp hair ICP-DRC-MS analysis. *J. Trace Elem. Med. Biol.* **2018**, *50*, 658–663. [CrossRef]
14. Wang, Q.; Sun, H.; Jin, L.; Wang, W.; Zhang, Z.; Chen, Y. A novel turn on and reversible sensor for Al^{3+} and its applications in bioimaging. *J. Lumin.* **2018**, *203*, 113–120. [CrossRef]
15. Lima, L.C.; Papai, R.; Gaubeur, I. Butan-1-ol as an extractant solvent in dispersive liquid-liquid microextraction in the spectrophotometric determination of aluminium. *J. Trace Elem. Med. Biol.* **2018**, *50*, 175–181. [CrossRef]
16. Mohseni, H.K.; Matysiak, W.; Chettle, D.R.; Byun, S.H.; Priest, N.; Atanackovic, J.; Prestwich, W.V. Optimization of data analysis for the in vivo neutron activation analysis of aluminum in bone. *Appl. Radiat. Isot.* **2016**, *116*, 34–40. [CrossRef]
17. Ziola-Frankowska, A.; Kuta, J.; Frankowski, M. Application of a new HPLC-ICP-MS method for simultaneous determination of Al^{3+} and aluminium fluoride complexes. *Heliyon* **2015**, *1*, e00035. [CrossRef] [PubMed]
18. Suherman, A.L.; Tanner, E.E.; Kuss, S.; Sokolov, S.V.; Holter, J.; Young, N.P.; Compton, R.G. Voltammetric determination of aluminium (III) at tannic acid capped-gold nanoparticle modified electrodes. *Sens. Actuators B Chem.* **2018**, *265*, 682–690. [CrossRef]
19. Ramezani, S.; Jahani, R.; Mashhadizadeh, M.H.; Shahbazi, S.; Jalilian, S. A novel ionic liquid/polyoxomolybdate based sensor for ultra-high sensitive monitoring of Al(III): Optimization by Taguchi statistical design. *J. Electroanal. Chem.* **2018**, *814*, 7–19. [CrossRef]
20. Bai, J.; Zhang, X.; Peng, Y.; Hong, X.; Liu, Y.; Jiang, S.; Ning, B.; Gao, Z. Ultrasensitive sensing of diethylstilbestrol based on AuNPs/MWCNTs-CS composites coupling with sol-gel molecularly imprinted polymer as a recognition element of an electrochemical sensor. *Sens. Actuators B Chem.* **2017**, *238*, 420–426. [CrossRef]
21. Janegitz, B.C.; Figueiredo-Filho, L.C.S.; Marcolino-Junior, L.H.; Souza, S.P.N.; Pereira-Filho, E.R.; Fatibello-Filho, O. Development of a carbon nanotubes paste electrode modified with crosslinked chitosan for cadmium(II) and mercury(II) determination. *J. Electroanal. Chem.* **2011**, *660*, 209–216. [CrossRef]
22. Mergen, Ö.B.; Arda, E. Determination of Optical Band Gap Energies of CS/MWCNT Bio-nanocomposites by Tauc and ASF Methods. *Synth. Met.* **2020**, *269*, 116539. [CrossRef]
23. Bolat, E.Ö.; Tığ, G.A.; Pekyardımcı, Ş. Fabrication of an amperometric acetylcholine esterase-choline oxidase biosensor based on MWCNTs-Fe₃O₄NPs-CS nanocomposite for determination of acetylcholine. *J. Electroanal. Chem.* **2017**, *785*, 241–248. [CrossRef]
24. Mu, Z.; Ma, L.; Wang, J.; Zhou, J.; Yuan, Y.; Bai, L. A target-induced amperometric aptasensor for sensitive zearalenone detection by CS@AB-MWCNTs nanocomposite as enhancers. *Food Chem.* **2021**, *340*, 128128. [CrossRef]
25. Abedi, A.; Bakhshandeh, B.; Babaie, A.; Mohammadnejad, J.; Vahdat, S.; Mombeiny, R.; Moosavi, S.R.; Amini, J.; Tayebi, L. Concurrent application of conductive biopolymeric chitosan/ polyvinyl alcohol/ MWCNTs nanofibers, intracellular signaling manipulating molecules and electrical stimulation for more effective cardiac tissue engineering. *Mater. Chem. Phys.* **2021**, *258*, 123842. [CrossRef]
26. Parvizifard, M.; Karbasi, S. Physical, mechanical and biological performance of PHB-Chitosan/MWCNTs nanocomposite coating deposited on bioglass based scaffold: Potential application in bone tissue engineering. *Int. J. Biol. Macromol.* **2020**, *152*, 645–662. [CrossRef] [PubMed]
27. Ren, Z.; Luo, Y.; Liu, X.; Zhang, J.; Chen, S.; Yu, R.; Xu, Y.; Meng, Z.; Li, J.; Ma, Y.; et al. Preparation, characterization and controlled-release property of CS crosslinked MWCNT based on Hericium erinaceus polysaccharides. *Int. J. Biol. Macromol.* **2020**, *153*, 1310–1318. [CrossRef] [PubMed]

28. Shalauddin, M.; Akhter, S.; Bagheri, S.; Abd Karim, M.S.; Adib Kadri, N.; Basirun, W.J. Immobilized copper ions on MWCNTS-Chitosan thin film: Enhanced amperometric sensor for electrochemical determination of diclofenac sodium in aqueous solution. *Int. J. Hydrogen Energy* **2017**, *42*, 19951–19960. [[CrossRef](#)]
29. Zhao, W.R.; Kang, T.F.; Lu, L.P.; Cheng, S.Y. Electrochemical magnetic imprinted sensor based on MWCNTs@CS/CTABr surfactant composites for sensitive sensing of diethylstilbestrol. *J. Electroanal. Chem.* **2018**, *818*, 181–190. [[CrossRef](#)]
30. Chen, Y.; Sun, Y.; Waterhouse, G.I.; Gao, H.; Xu, Z. Highly selective molecularly imprinted gel-based electrochemical sensor with CuS@ COOH-MWCNTs signal amplification for simultaneous detection of vanillin and tartrazine in foods. *Sens. Actuators B Chem.* **2023**, *377*, 133045. [[CrossRef](#)]
31. Zhang, L.; Sun, M.; Jing, T.; Li, S.; Ma, H. A facile electrochemical sensor based on green synthesis of Cs/Ce-MOF for detection of tryptophan in human serum. *Colloids Surf. A Physicochem. Eng. Asp.* **2022**, *648*, 129225. [[CrossRef](#)]
32. Komkova, M.A.; Pasquarelli, A.; Andreev, E.A.; Galushin, A.A.; Karyakin, A.A. Prussian Blue modified boron-doped diamond interfaces for advanced H₂O₂ electrochemical sensors. *Electrochim. Acta* **2020**, *339*, 135924. [[CrossRef](#)]
33. Yang, S.; Zhao, J.; Tricard, S.; Yu, L.; Fang, J. A sensitive and selective electrochemical sensor based on N, P-Doped molybdenum Carbide@Carbon/Prussian blue/graphite felt composite electrode for the detection of dopamine. *Anal. Chim. Acta* **2020**, *1094*, 80–89. [[CrossRef](#)] [[PubMed](#)]
34. Ruggeri, S.; Terzi, F.; Zanfognini, B.; Corsi, E.; Dossi, N.; Zanardi, C.; Pigani, L.; Seeber, R. Electroanalytical determination of soluble Mn(II) species at high concentration levels. *Electrochim. Acta* **2017**, *240*, 108–113. [[CrossRef](#)]
35. Zuziak, J.; Jakubowska, M. Voltammetric determination of aluminum-Alizarin S complex by renewable silver amalgam electrode in river and waste waters. *J. Electroanal. Chem.* **2017**, *794*, 49–57. [[CrossRef](#)]
36. Jeon, W.Y.; Kim, H.S.; Jang, H.W.; Lee, Y.S.; Shin, U.S.; Kim, H.H.; Choi, Y.B. A stable glucose sensor with direct electron transfer, based on glucose dehydrogenase and chitosan hydro bonded multi-walled carbon nanotubes. *Biochem. Eng. J.* **2022**, *187*, 108589. [[CrossRef](#)]
37. Ringgit, G.; Siddiquee, S.; Saallah, S.; Mohamad Lal, M.T. Optimisation of an Electrochemical Sensor Based on Bare Gold Electrode for Detection of Aluminium Ion. *Borneo Int. J. Biotechnol.* **2020**, *1*, 103. [[CrossRef](#)]
38. Diaconu, M.; Litescu, S.C.; Radu, G.L. Laccase–MWCNT–chitosan biosensor—A new tool for total polyphenolic content evaluation from in vitro cultivated plants. *Sens. Actuators B Chem.* **2010**, *145*, 800–806. [[CrossRef](#)]
39. Siddiquee, S.; Yusof, N.A.; Salleh, A.B.; Tan, S.G.; Bakar, F.A. Electrochemical DNA biosensor for the detection of *Trichoderma harzianum* based on a gold electrode modified with a composite membrane made from an ionic liquid, ZnO nanoparticles and chitosan, and by using acridine orange as a redox indicator. *Microchim. Acta* **2011**, *172*, 357–363. [[CrossRef](#)]
40. Geng, L.; Huang, J.; Zhai, H.; Shen, Z.; Han, J.; Yu, Y.; Fang, H.; Li, F.; Sun, X.; Guo, Y. Molecularly imprinted electrochemical sensor based on multi-walled carbon nanotubes for specific recognition and determination of chloramphenicol in milk. *Microchem. J.* **2022**, *182*, 107887. [[CrossRef](#)]
41. Jin, M.; Zhang, X.; Zhen, Q.; He, Y.; Chen, X.; Lyu, W.; Han, R.; Ding, M. An electrochemical sensor for indole in plasma based on MWCNTs-chitosan modified screen-printed carbon electrode. *Biosens. Bioelectron.* **2017**, *98*, 392–397. [[CrossRef](#)] [[PubMed](#)]
42. Arvand, M.; Kermanian, M. Potentiometric determination of aluminum in foods, pharmaceuticals, and alloys by AIMCM-41-modified carbon paste electrode. *Food Anal. Methods* **2013**, *6*, 578–586. [[CrossRef](#)]
43. Mashhadizadeh, M.H.; Khani, H. Sol-Gel-Au nano-particle modified carbon paste electrode for potentiometric determination of sub ppb level of Al (III). *Anal. Methods* **2010**, *2*, 24–31. [[CrossRef](#)]
44. Saleh, M.B.; Hassan, S.S.; Gaber, A.A.A.; Kream, N.A.A. Novel potentiometric membrane sensor for selective determination of aluminum (III) ions. *Anal. Chim. Acta* **2001**, *434*, 247–253. [[CrossRef](#)]
45. Qiong, L.; Lirong, W.; Danli, X.; Guanghan, L. Determination of trace aluminum in foods by stripping voltammetry. *Food Chem.* **2006**, *97*, 176–180. [[CrossRef](#)]
46. Kyriakopoulos, G.; Doulia, D.; Hourdakos, A. Effect of ionic strength and pH on the adsorption of selected herbicides on Amberlite. *J. Environ. Anal. Chem.* **2006**, *86*, 207–214. [[CrossRef](#)]
47. Arancibia, V.; Munoz, C. Determination of aluminium in water samples by adsorptive cathodic stripping voltammetry in the presence of pyrogallol red and a quaternary ammonium salt. *Talanta* **2007**, *73*, 546–552. [[CrossRef](#)] [[PubMed](#)]
48. Chaiyo, S.; Mehmeti, E.; Žagar, K.; Siangproh, W.; Chailapakul, O.; Kalcher, K. Electrochemical sensors for the simultaneous determination of zinc, cadmium and lead using a Nafion/ionic liquid/graphene composite modified screen-printed carbon electrode. *Anal. Chim. Acta* **2016**, *918*, 26–34. [[CrossRef](#)]
49. Lee, S.; Oh, J.; Kim, D.; Piao, Y. A sensitive electrochemical sensor using an iron oxide/graphene composite for the simultaneous detection of heavy metal ions. *Talanta* **2016**, *160*, 528–536. [[CrossRef](#)]
50. Bard, A.J.; Faulkner, L.R.; White, H.S. *Electrochemical Methods: Fundamentals and Applications*; John Wiley & Sons: Hoboken, NJ, USA, 2022.
51. Arvand, M.; Asadollahzadeh, S.A. Ion-selective electrode for aluminum determination in pharmaceutical substances, tea leaves and water samples. *Talanta* **2008**, *75*, 1046–1054. [[CrossRef](#)] [[PubMed](#)]
52. Bohari, N.A.; Siddiquee, S.; Saallah, S.; Misson, M.; Arshad, S.E. Electrochemical behaviour of real-time sensor for determination mercury in cosmetic products based on PANI/MWCNTs/AuNPs/ITO. *Cosmetics* **2021**, *8*, 17. [[CrossRef](#)]

53. Asiri, A.M.; Hussain, M.M.; Arshad, M.N.; Rahman, M.M. Sensitive and selective heavy metal ion, Mn^{2+} sensor development based on the synthesized (E)-N'-chlorobenzylidene-benzenesulfonohydrazide (CBBSH) molecules modified with nafion matrix. *J. Ind. Eng. Chem.* **2018**, *63*, 312–321. [[CrossRef](#)]
54. Sun, Y.; He, X.; Ji, J.; Jia, M.; Wang, Z.; Sun, X. A highly selective and sensitive electrochemical CS-MWCNTs/Au-NPs composite DNA biosensor for *Staphylococcus aureus* gene sequence detection. *Talanta* **2015**, *141*, 300–306. [[CrossRef](#)]
55. Dorraji, P.S.; Jalali, F. Novel sensitive electrochemical sensor for simultaneous determination of epinephrine and uric acid by using a nanocomposite of MWCNTs–chitosan and gold nanoparticles attached to thioglycolic acid. *Sens. Actuators B Chem.* **2014**, *200*, 251–258. [[CrossRef](#)]
56. Sun, L.; Yang, M.; Guo, H.; Zhang, T.; Wu, N.; Wang, M.; Yang, F.; Zhang, J.; Yang, W. COOH-MWCNT connected COF and chemical activated CTF as a novel electrochemical sensing platform for simultaneous detection of acetaminophen and p-aminophenol. *Colloids Surf. A Physicochem. Eng. Asp.* **2022**, *647*, 129092. [[CrossRef](#)]
57. Roushani, M.; Bakyas, K.; Dizajdizi, B.Z. Development of sensitive amperometric hydrogen peroxide sensor using a CuNPs/MB/MWCNT-C60-Cs-IL nanocomposite modified glassy carbon electrode. *Mater. Sci. Eng. C.* **2016**, *64*, 54–60. [[CrossRef](#)] [[PubMed](#)]
58. Rezaei, B.; Jamei, H.R.; Ensafi, A.A. An ultrasensitive and selective electrochemical aptasensor based on rGO-MWCNTs/Chitosan/carbon quantum dot for the detection of lysozyme. *Biosens. Bioelectron.* **2018**, *115*, 37–44. [[CrossRef](#)]
59. Kefala, G.; Economou, A.; Sofoniou, M. Determination of trace aluminium by adsorptive stripping voltammetry on a preplated bismuth-film electrode in the presence of cupferron. *Talanta* **2006**, *68*, 1013–1019. [[CrossRef](#)] [[PubMed](#)]
60. Gupta, V.K.; Jain, A.K.; Maheshwari, G. Aluminum (III) selective potentiometric sensor based on morin in poly (vinyl chloride) matrix. *Talanta* **2007**, *72*, 1469–1473. [[CrossRef](#)]
61. Zhang, F.; J6i, M.; Xu, Q.; Yang, L.; Bi, S. Linear scan voltammetric indirect determination of AlIII by the catalytic cathodic response of norepinephrine at the hanging mercury drop electrode. *J. Inorg. Biochem.* **2005**, *99*, 1756–1761. [[CrossRef](#)]
62. Santos, L.B.; de Souza, M.T.; Paulino, A.T.; Garcia, E.E.; Nogami, E.M.; Garcia, J.C.; de Souza, N.E. Determination of aluminum in botanical samples by adsorptive cathodic stripping voltammetry as Al-8-hydroxyquinoline complex. *Microchem. J.* **2014**, *112*, 50–55. [[CrossRef](#)]
63. Abbaspour, A.; Esmailbeig, A.R.; Jarrahpour, A.A.; Khajeh, B.; Kia, R. Aluminium (III)-selective electrode based on a newly synthesized tetradentate Schiff base. *Talanta* **2002**, *58*, 397–403. [[CrossRef](#)] [[PubMed](#)]
64. Gyamfi, E.; Appiah-Adjei, E.K.; Adjei, K.A. Potential heavy metal pollution of soil and water resources from artisanal mining in Kokoteasua, Ghana. *Groundw. Sustain. Dev.* **2019**, *8*, 450–456. [[CrossRef](#)]
65. Kumar, M.; Nagdev, R.; Tripathi, R.; Singh, V.B.; Ranjan, P.; Soheb, M.; Ramanathan, A.L. Geospatial and multivariate analysis of trace metals in tubewell water using for drinking purpose in the upper Gangetic basin, India: Heavy metal pollution index. *Groundw. Sustain. Dev.* **2019**, *8*, 122–133. [[CrossRef](#)]

Disclaimer/Publisher's Note: The statements, opinions and data contained in all publications are solely those of the individual author(s) and contributor(s) and not of MDPI and/or the editor(s). MDPI and/or the editor(s) disclaim responsibility for any injury to people or property resulting from any ideas, methods, instructions or products referred to in the content.